Numerical method to model the creep of recycled aggregate concrete by considering the old attached mortar

Menghuan Guo, Frédéric Grondin, Ahmed Loukili

Numerical method to model the creep of recycled aggregate concrete by considering the old attached mortar

Menghuan Guo, Frédéric Grondin, Ahmed Loukili

Institut de Recherche en Génie Civil et Mécanique, GeM-UMR 6183, Centrale Nantes-Université de Nantes-CNRS, 1 rue de la Noë, BP 92101, 44321 Nantes, France

Abstract

Experimental creep tests have shown that recycled aggregate in concrete increases its displacement rate. In order to explore this behavior, multiscale modeling has been performed. To consider the old attached mortar surrounding recycled aggregates, creep parameters were calculated from the cement hydrates scale. Sixteen ordinary mortars were calculated to have a large range of values. A homogenization model was applied to calculate the viscoelastic properties. At the concrete scale, in order to take into account the influence of the heterogeneity of the recycled material, a creep-damage coupling model was used. The proposed numerical method demonstrates that the viscoelastic strain of recycled aggregates is not negligible, and leads to a larger creep displacement and higher damage level. Its influence on the time-dependent behavior of recycled aggregate concrete should be considered in modeling.

Keywords:

Recycled aggregate concrete, Old mortar, Modelling, Creep, Viscoelastic

1. Introduction

In the 21st century, the concept of sustainable development prompts the reutilization of cement-based products derived from construction and demolition waste. Concrete made by partially or completely substituting recycled aggregates (RAs) for natural aggregates represents an environmentally friendly material that holds the promise of recycling construction waste. Extensive research work has been carried out to study the workability and mechanical properties of recycled aggregate concrete (RAC) with the purpose of extending its application for structural use [1–7]; fruitful results

Email addresses: Menghuan.Guo@ec-nantes.fr (Menghuan Guo), Frederic.Grondin@ec-nantes.fr (Frédéric Grondin), Ahmed.Loukili@ec-nantes.fr (Ahmed Loukili)

Preprint submitted to Cement and Concrete Research *November 29, 2018*

have been achieved. However, research concerning the durability-related performance of recycled concrete has until now been limited. In particular, the creep behavior of structural RAC has not yet been fully studied, despite the fact that creep is of considerable importance for the structural design of concrete.

As we all know, the creep deformation of normal concrete is a complex time-dependent phenomenon influenced by several factors, including the mix design, temperature and relative humidity, load conditions and size of the structure [8, 9]. In the case of RAC, this phenomenon becomes much more complicated. Generally, the incorporation of RAs leads to accelerated concrete creep, the magnitude of which, all other things being equal, depends on the aggregates' quality and replacement ratio [10, 11]. Domingo-Cabo et al. [12] reported that when 100 % coarse natural aggregate was replaced with RAs, there was a 51 % increase in the creep deformation as compared to that experienced by the control concrete. According to Seara-Paz et al. [13], the specific creep of recycled concrete is higher than that of conventional concrete, with the increment ranging from 51 % to 73 %. Tam et al. [14] experimentally investigated the drying creep behavior of concrete made with varied RA replacement ratios of 0 %, 30 %, 50 %, 70 % and 100 %, and concluded that drying creep increases with the replacement ratios. Wang et al. [15] also demonstrated that the long-term deflections of composite concrete slabs increase with the RA substitution ratio. Similar results are reported by [16–20].

As observed by several researchers mentioned above, the increased deformation by creep is directly related to the attached old mortar surrounding the aggregate particles. The old residual mortar is usually porous and contains microcracks [21, 22], due to the prior mechanical crushing process. The content, elastic modulus and creep behavior of the old adhering mortar can greatly influence the RAC's creep characteristics [17, 20]. In order to account for this influence, Fan et al. [17] has adapted the Neville model to predict RAC creep with high accuracy. Likewise, Fathifazl and Razaqpur [23] have modified five rheological models for conventional concrete to make them suitable for application to RAC, with the effects of the quantity and properties of residual mortar on RAC creep delicately involved in the modification. Fathifazl et al. [24] also demonstrated that by applying the proposed "residual mortar factor" to the existing ACI and CEB

methods for calculating creep of conventional concrete, these methods could be also applied to predict RAC creep. Based on this proposed residual mortar factor, Wang et al. [15] has developed a homogeneous finite-element model to account for the time-dependent behavior of composite RAC slabs by including the effects of non-uniform shrinkage, creep and concrete cracking. Knaack and Kurama [16] concluded that the determined adjustment factors can be applied to existing natural aggregate concrete creep relationships (that is, code-based models) to predict the creep strains of RAC. Some of those authors [12, 13, 25–28] also put forward a set of correction factors for the creep coefficient of recycled concrete.

Generally, the aforementioned creep prediction methods are used either by proposing a creep coefficient to account for the amplified influence of recycled concrete, or by adding a residual mortar factor in existing creep models for conventional concrete. Both of these methods depend greatly on the experimental outcome. Several comparative studies have also been carried out [10, 28]. However, owing to the high scatter of old mortar properties and content, the application of these creep prediction models for RAC is quite limited. The available information on the effect of RAs on concrete creep does not allow a full understanding of their influence on the deformation of concrete structures. Thus the necessity of explicitly considering the effect of the properties of unknown old attached mortar on the creep prediction model is quite evident. Furthermore, a recent work [29] demonstrated that the resistance of recycled coarse aggregate to fragmentation is significantly lower than that of natural aggregate. The experimental results of [30–32] also showed that RAs tend to have higher water absorption, lower density and lower particle strength. It is vital that RA quality is evaluated in order to understand its role on the creep behavior of concrete [28]. In fact, analysis of the effects of all the existing phases in RAC on the creep behaviour of the material remains challenging. This study attempts to tackle this problem by carrying out a mesoscopic modeling of RAC. The RA mesh was generated explicitly in the finite element code Cast3M by considering the old original aggregate surrounded by the old attached mortar. RAs were distributed in a random way in concrete, and simulations of creep behavior were performed. A coupled creep-damage model [33] was used, and numerical results were analyzed and compared to experimental measurements.

As the characteristics of old attached mortar are unknown, we assumed that they were equivalent

to those of a set of traditional mortar. The methodology for the determination of the fracture properties of this set of chosen mortar has been presented in [3]. In this study, in order to characterise the time-dependent viscoelastic properties of the chosen mortar, an inverse analysis that allows the numerical model to upscale the phase characteristics to macroscopic properties of concrete was carried out [34]. A numerical homogenization method was applied for the calculation of the creep compliance between the different scales.

2. Experimental basis

In most cases, concrete structures are subjected to low load levels, which are generally inferior to 40 % of the material strength. It is generally accepted that in this loading range, the instantaneous mechanical behavior of concrete remains elastic and creep remains linear without damage occurring. It is very interesting to check whether RAC's creep compliance complies with the same practice. In this work, the RAC beams at the age of three months were loaded under a stress level of 40 % of the maximal resistance F_{max} for three months in order to evaluate the influence of the substitution ratio of RA for natural aggregate on the kinetics and amplitude of bending creep.

Concrete mixtures were prepared with CEM II/A-L 42.5N from Rochefort, crushed limestone aggregate and RA. RAs were obtained by crushing unknown waste concrete provided by one of the largest French recycling platforms (DLB de Gonesse), while the source concrete came from surrounding demolition sites. Therefore, the recycled materials used in this study represent the properties of a variety of collected waste from general construction and demolition sites. Variation of the RA replacement percentage (0, 30 % and 100 %) relative to the total mass of coarse aggregate in concrete mixtures was studied. All the mixtures were designed to have the same compressive strength in the range of 25-30 MPa and the same workability, according to the structural class S4 [8]. The studied mixtures are noted respectively: C-N-N - Concrete with Natural sand and Natural aggregate; C-N-30R - Concrete with Natural sand and 30 % Recycled aggregate; C-N-100R - Concrete with Natural sand and 100 % Recycled aggregate.

First, three-point bending tests were carried out on notched concrete beams with the dimensions of 100 × 200 × 800 mm^3 (b×h×L) at the age of 28 days [3]. F_{max} was thus determined according

to fracture tests controlled by the crack mouth opening displacement (CMOD). Flexural creep tests were then performed on frames with a capacity ranging from 5 to 50 kN (Figure 1) [35]. The load was applied by gravity with a weight and counterweight system, and the displacement was measured at midspan. All tests occurred in a climate-controlled chamber at 50 % of relative humidity and a temperature of 20 °C.

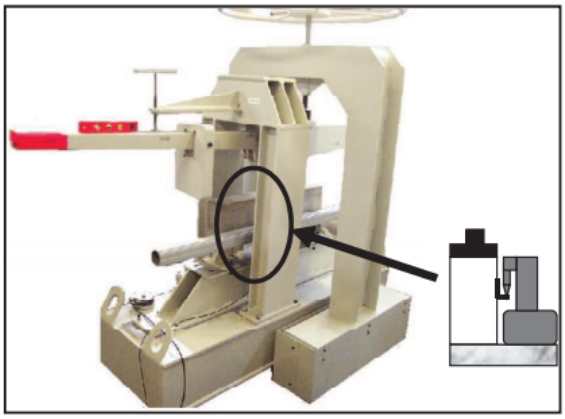

Figure 1: General view of the flexural creep frame.

For comparison between the three types of concrete that were studied, the specific delayed displacement was defined as the amount of deflection per unit applied stress. The stress was evaluated according to the following relationship:

$$\sigma = \frac{3}{4}\frac{\rho g h l^2}{(h-a_0)^2} + \frac{3}{2}\frac{Fl}{b(h-a_0)^2} \tag{1}$$

where ρ represents the density of concrete, l the distance between the two supports, F the applied force, h and b, respectively, the height and the width of the beam and a_0 the height of the notch. After subtracting the instantaneous response, the specific creep displacement was obtained.

Figure 2 presents the specific delayed displacements for the three concrete types. Note that the creep kinetics were comparable for natural aggregate concrete and 30 % RAC, with an amplitude 1.2 times greater after three months of loading for the latter one. For concrete with 100 % RA, creep developed faster and the amplitude was practically 1.6 times greater than normal concrete. The creep displacement of normal concrete, after three months of loading, is reached by C-N-100R

after only four weeks of loading. These results agree with the previous work of other researchers [12–14]. The fracture analysis of these three types of concrete [3, 36] offers two assumptions: either RA creeps, or microcracks initiate and weaken the concrete that is subjected to constant load. For the purpose of checking these two assumptions, we analyzed the creep evolution by calculating the ratio of the specific delayed displacement at time t to the final specific displacement measured at the end of the test, as shown in Figure 3.

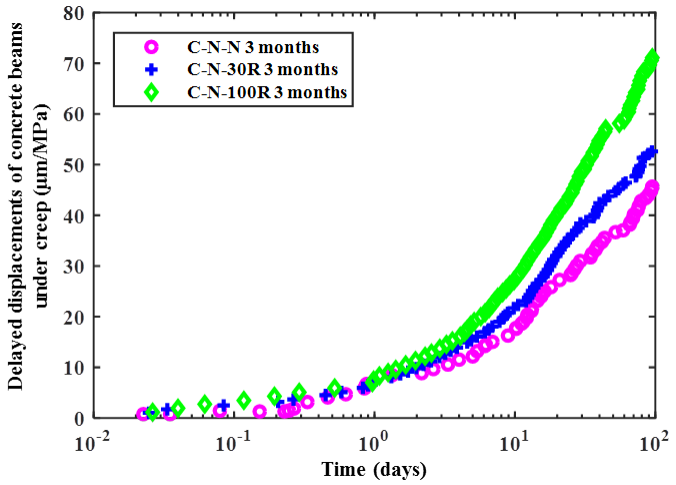

Figure 2: Delayed displacements of concrete beams under creep.

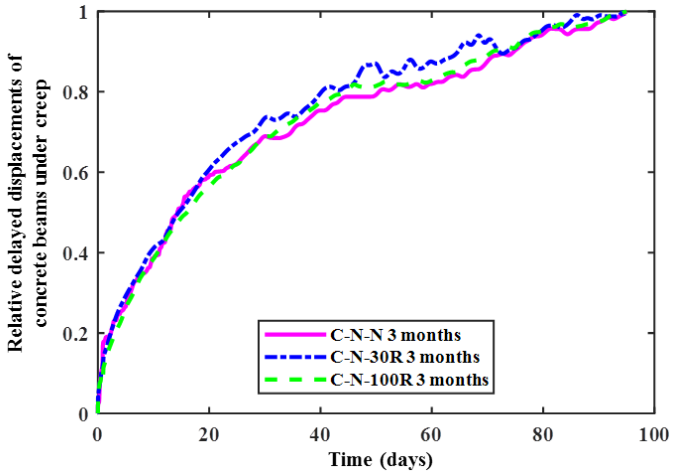

Figure 3: Relative delayed displacements of concrete beams under creep.

Note that the delayed displacement amplitudes were quite different for the three kinds of concrete. Nevertheless, the evolution trend of the relative delayed displacement was comparable for the three concrete types, which suggests that the creep mechanism was identical for recycled concrete and normal concrete. In other words, viscoelasticity and/or microcracks were of the same type in the three kinds of concrete though their amplitudes were different. In brief, the experimental tests performed in this work show clearly the effect of RA on the creep behavior of concrete. However, these tests were time-limited. It is imperative that a creep prediction model that considers all the involved mechanisms be built in order to prevent recycled concrete structures from cracking at an early age as well as in the long term, and to quantify, at the first time, the degradation of their properties.

3. Description of the representative specimens for multiscale modeling

The model used here is based on the assumption that the creep of concrete depends mainly on that of calcium silicate hydrates (C-S-H) [34]. According to Smilauer et al. [37], C-S-H is the only phase that is responsible for creep at the cement paste scale and at the concrete scale. The experimental study of Torrenti et al. [38] showed that the derivative of the basic creep compliance with respect to the loading time is unique whatever the loading age. Others researchers [39–41] have also concluded that the creep of cement paste originates in C-S-H. All of them confirm the hypothesis made in the multi-scale model used here. In this model, in order to calculate the creep defined by a volume of material with a viscoelastic matrix and elastic inclusions, four scales are considered:

- Sub-microscopic, corresponding to the C-S-H scale, represented by a homogeneous C-S-H matrix and the pores as inclusions
- Microscopic, corresponding to the cement paste scale, represented by a homogeneous matrix equivalent to the material of the sub-microscopic scale and the hydration products other than C-S-H and the residual cement clinkers as inclusions

- Sub-mesoscopic, corresponding to the mortar scale, represented by a homogeneous matrix equivalent to the cement paste and the grains of sand as inclusions

- Mesoscopic, corresponding to the concrete scale, represented by a homogeneous matrix equivalent to the mortar and the aggregates as inclusions

In this study, an effective interphase (EI) between aggregate and cement mortar was added and considered in the modeling [42]. Thus at the concrete scale, a three-point bending beam with a mesoscopic mesh generated in the central part of the beam was simulated so as to take into account the heterogeneity of the material, i.e. the aggregate, cement mortar and EI. For the rest, a homogeneous mesh with a gradually larger element toward the end of the beam was incorporated in order to avoid stress concentration. The macroscopic properties of those two parts were considered to be the same as for concrete. A constant load of 40 % of the maximal strength was applied to the rigid plate (linearly elastic law) fixed at the top middle of the beam (Figure 4). For the other two scales, the simulation of a representative elementary volume (REV) in direct tension was carried out; a uniaxial loading was applied to the upper side of the REV while the vertical displacement of the lower side of the REV was constrained. In order to ensure the stability of the volume and to comply with minimum dimension conditions, the size of a REV must be at least equal to four times the diameter of the largest inclusion and the finite element size should be less than or equal to 0.8 times the diameter of the smallest inclusion [43]. Here, at the mortar scale the REV was 10×10 mm^2 and at the cement paste scale the REV was 300×300 µm^2. As concrete structures are brittle in tension, the tensile cracking was predominant in the flexural test. At the lower scales, constant tensile loads were applied on mortar and cement paste specimens and only the effective part of the compliance in the loading axis was considered. The other deformations showed negligible values. Thus, the homogenization calculations were performed only in 2D. In the case of massive concrete structures, 3D calculations are recommended, but they were not studied in this work.

To simplify the modeling at the cement paste scale, only one type of particle with a single size was used to represent the inclusions. Its elastic properties were calculated by averaging the elastic

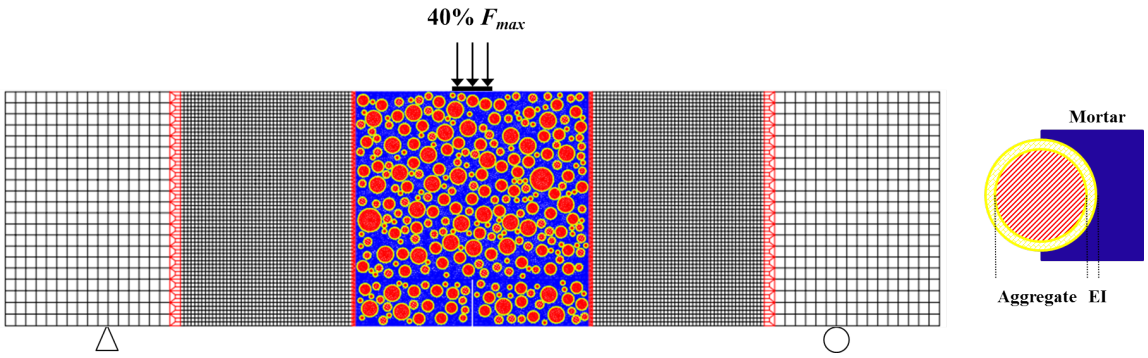

Figure 4: Meshing and boundary conditions of the concrete beam for a three-point bending creep test.

characteristics of the hydrates (CH, ettringite, gypsum, C_3AH_6, FH_3) and the residual cement phases (C_3S, C_2S, C_3A, C_4AF), with the set forming a volume denoted by $V_{hy-clinker}$. For mortar scale, the experimental size distribution of sand grains was used. For concrete scale, the aggregate size distribution in the modelling was defined according to the experimental value for the three kinds of concrete (Table 1).

Table 1: Inclusion size distribution for each scale (ϕ - diameter and V_f - volume fraction).

Cement paste	ϕ (mm)	0.03							
	V_f (%)	30							
Mortar	ϕ (mm)	0.1875	0.375	0.75	1.5	2.4	3.4	4.8	
	V_f (%)	4	10	15	13	4	3	1	
Concrete	ϕ (mm)	4	6.3	7.1	10	14	20		
(C-N-N)	V_f (%)	3	5	4	16	13	2		
Concrete	ϕ (mm)	**5**	**6.3**	**8**	**10**	**12.5**	**16**	**20**	
(C-N-100**R**)	V_f (%)	**2.8**	**4.3**	**2.1**	**9.6**	**10.5**	**8**	**1.8**	
Concrete	ϕ (mm)	6.3	**10**	10	**12.5**	14	**16**	**20**	20
(C-N-30**R**)	V_f (%)	4	**2**	7	**4**	8	**5**	**4**	7

For each scale, the mesh generation of the mesoscopic part was conducted with the algorithm developed by Mounajed [43, 44]. It consisted of generating a volume by introducing a random distribution of the various inclusions of different sizes in a solid matrix. Note that the third interphase

surrounding aggregate was introduced only for the concrete scale [42].

The distribution algorithm generated random positions of the inclusion gravity centres in the interested area of the volume. At this step, an inclusion i was formed by an aggregate with a surrounding interphase. The unit volume of this inclusion of type i was calculated as follows:

$$\begin{cases} V_{inclusion} = \pi R_i^2 & \text{in cement paste and mortar} \\ V_{inclusion} = \pi (R_i + \delta_{EI})^2 & \text{in concrete} \end{cases} \tag{2}$$

where R_i is the inclusion radius of type i and δ_{EI} the thickness of EI.

A test was conducted to check that two inclusions did not overlap. The distance between the gravity center of an existing inclusion with a radius of R_1 and that of a candidate inclusion with a radius of R_2 should be higher than the distance d_{min} defined as:

$$d_{min} = R_1 + R_2 \tag{3}$$

After the validation of the inclusions' position, the elements were assigned with material characteristics. First, all the elements were defined as having the matrix properties. Then, the model assigned different material properties to the elements by checking the distance d_{vef} between the gravity center of the element and that of the inclusion:

- If $d_{vef} \leq R_i$ the inclusion properties
- If $R_i < d_{vef} \leq R_i + \delta_{EI}$ the EI properties (only in concrete)
- If $d_{vef} > R_i\,(+\delta_{EI})$ the matrix properties

4. The problem formulation

4.1. Creep-damage coupling model

A volume V of concrete was formed by three media: a matrix defined by the medium V_m, inclusions defined by the medium V_i and at the concrete scale EI around the inclusions defined by the medium V_{EI}. A constant force $\bar{F}$ was applied on one of the surface boundary Γ_1 with the unit

normal vector $\bar{n}$. This load implied local displacement fields $\bar{u}(\bar{y})$, local strain fields $\bar{\bar{\varepsilon}}(\bar{y})$ and local stress fields $\bar{\bar{\sigma}}(\bar{y})$ in each point $\bar{y}$ of V.

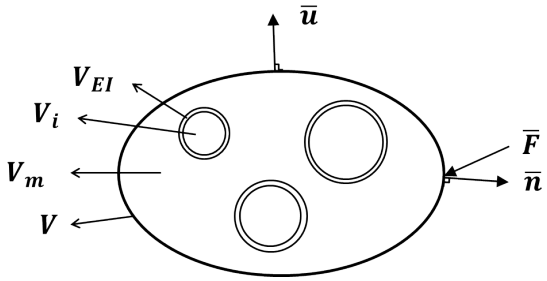

Figure 5: Illustration of the the mechanical problem.

The non-linear elastic problem was written as follows:

$$\overline{div}\bar{\bar{\sigma}}(\bar{y}) = \bar{0} \quad \forall \bar{y} \in V \tag{4}$$

$$\bar{\bar{\sigma}}(\bar{y}) = \bar{\bar{\bar{\bar{C}}}}(\bar{y}, \bar{\bar{\varepsilon}}(\bar{y})) : (\bar{\bar{\varepsilon}}(\bar{y}) - \bar{\bar{\varepsilon}}^v(\bar{y})) \quad \forall \bar{y} \in V \tag{5}$$

$$\bar{\bar{\varepsilon}}(\bar{y}) = \frac{1}{2}\left(\bar{\bar{\nabla}}\bar{u}(\bar{y}) + {}^t\bar{\bar{\nabla}}\bar{u}(\bar{y})\right) \quad \forall \bar{y} \in V \tag{6}$$

$$\bar{F} = \bar{\bar{\sigma}} \cdot \bar{n} \quad \forall \bar{y} \in \Gamma_1 \tag{7}$$

$$\bar{u} = \bar{U} \quad \forall \bar{y} \in \Gamma_2 \tag{8}$$

where $\bar{\bar{\bar{\bar{C}}}}(\bar{y}, \bar{\bar{\varepsilon}}(\bar{y}))$ represents the secant stiffness tensor depending on the local strains and damage, $\bar{\bar{\varepsilon}}^v(\bar{y})$ the local viscoelastic strain fields and Γ_2 the boundary of V on which macroscopic displacements conditions were applied.

The isotropic damage model developed by Fichant et al. [45] was chosen for this study. For the isotropic version of the model, the relationship between effective stress and total stress is given by [46]:

$$\bar{\bar{\sigma}}(\bar{y}) = (1-d)\bar{\bar{\tilde{\sigma}}}(\bar{y}) \tag{9}$$

where d represents the scalar value of the isotropic damage that depends only on the equivalent strain calculated according to the positive part $((\cdot)_+)$ of the elastic strain tensor $\bar{\bar{\varepsilon}}^e(\bar{y})$:

$$\bar{\bar{\varepsilon}}_{eq} = \sqrt{(\bar{\bar{\varepsilon}}^e)_+ : (\bar{\bar{\varepsilon}}^e)_+} \tag{10}$$

The evolution of the damage variable, due to external mechanical loads, was an exponential form:

$$d = 1 - \frac{\varepsilon_{d0}}{\varepsilon_{eq}} \exp[B_t(\varepsilon_{d0} - \varepsilon_{eq})] \tag{11}$$

where B_t represents a damage parameter to control the slope of the strain softening constitutive relation in function of the width h of the element and ε_{d0} the strain threshold.

The viscoelastic strain was defined as the sum of the elementary strains associated with each chain of the generalized Kelvin-Voigt model:

$$\bar{\bar{\varepsilon}}^v(t) = \sum_{i=1}^{4} \bar{\bar{\varepsilon}}_v^i(t) \tag{12}$$

For each chain i the viscoelastic strain $\bar{\bar{\varepsilon}}_v^i(t)$ was the solution of a first order nonlinear differential equation:

$$\eta^i \dot{\bar{\bar{\varepsilon}}}_v^i(t) + k^i \bar{\bar{\varepsilon}}_v^i(t) = \bar{\bar{\sigma}}(t) \tag{13}$$

where k^i was the stiffness and η^i the viscosity of the Kelvin-Voigt unit.

The total viscoelastic strain was calculated by summing all the elementary viscoelastic strains, and the latter were obtained by solving analytically the differential equations:

$$\Delta\bar{\varepsilon}_v^{n+1} = \bar{\varepsilon}_v^{n+1} - \bar{\varepsilon}_v^n = a_v \bar{\varepsilon}_v^n + b_v \bar{\sigma}_n + c_v \bar{\sigma}_{n+1} \tag{14}$$

where $\bar{\varepsilon}_v^n$ represents the viscoelastic strain vector at the time step n and a_v, b_v, c_v are the material parameters [47].

In fact, the viscoelastic strain field was related to the stress field by the creep compliance $\bar{\bar{\bar{\bar{J}}}}(t)$ such that:

$$\bar{\bar{\varepsilon}}^{v}(t,\bar{y}) = \bar{\bar{\bar{\bar{J}}}}(t) : \bar{\bar{\sigma}}(t,\bar{y}) \tag{15}$$

For a 2D model, the compliance tensor $\bar{\bar{\bar{\bar{J}}}}(t)$ was defined by three components: $J_{1111}(t)$, $J_{2222}(t)$ and $J_{1212}(t)$, corresponding respectively to the compliance in the loading axis, in the axis perpendicular to the loading and in the transverse axis. According to the generalized Kelvin model $J_{ijkl}(t)$ is defined as follows:

$$J_{ijkl}(t) = \frac{1}{E(t)} + \sum_{p=1}^{3} \frac{1}{k^{p}_{ijkl}(t)} (1 - e^{\frac{-t}{\tau^{p}_{ijkl}}}) \tag{16}$$

where E(MPa) is the elastic modulus, k^{p}_{ijkl}(MPa) is the stiffness of the Kelvin unit and τ^{p}_{ijkl}(s) is the characteristic time.

In order to realize the creep compliance transformation between the different scales, a numerical homogenization method [34] of the creep compliance was applied.

4.2. Numerical homogenization method

According to Grondin [48] for a bi-phase REV the solving of an elastic homogenization problem is equivalent to the solving of problems (equations (4)-(8)) at each time step t^{p} of the time discretization interval $t^{0} = 0, t^{1}, ..., t^{p}, ..., t^{n} = t^{max}$. The tensor relating the strain field and the stress field is constant at the computation time t^{p}, such that:

$$\left\langle \bar{\bar{\varepsilon}}^{v}(t^{p},\bar{y}) \right\rangle_{V} = \bar{\bar{\bar{\bar{J}}}}^{hom}(t^{p}) : \left\langle \bar{\bar{\sigma}}(t^{p},\bar{y}) \right\rangle_{V} \tag{17}$$

The final creep compliance is the integral of $\bar{\bar{\bar{\bar{J}}}}^{hom}(t^{p})$ with respect to time. The applied stress can be described by considering only the time-dependent stresses:

$$\left\langle \bar{\bar{\sigma}}(t,\bar{y}) \right\rangle_{V} = H(t) \left\langle \bar{\bar{\sigma}}^{0} \right\rangle_{V} \tag{18}$$

where $H(t)$ is the Heaviside function:

$$\begin{cases} H(t) = 0 \quad \text{if} \quad t = 0 \\ H(t) = 1 \quad \text{if} \quad t > 0 \end{cases} \tag{19}$$

By summing the components of the constant elementary tensors with respect to time, the formula (17) becomes:

$$\sum_{p=0}^{p=n} \left\langle \varepsilon_{ij}^{v}(t^p, \bar{y}) \right\rangle_v = \sum_{p=0}^{p=n} J_{ijkl}^{hom}(t^p) \left\langle \sigma_{kl}(t^p) \right\rangle_V \tag{20}$$

By using the expression (18), the preceding formula is written:

$$\sum_{p=0}^{p=n} \left\langle \varepsilon_{ij}^{v}(t^p, \bar{y}) \right\rangle_v = \sum_{p=0}^{p=n} J_{ijkl}^{hom}(t^p) H(t^p) \left\langle \sigma_{kl}^{0} \right\rangle_V \tag{21}$$

Through replacing $H(t^p)$ by its expression and considering that the strain is zero at $t = 0$, one obtains:

$$\left\langle \varepsilon_{ij}^{v}(t, \bar{y}) \right\rangle_V = J_{ijkl}^{hom}(t) \left\langle \sigma_{kl}(t) \right\rangle_V \tag{22}$$

It should be highlighted that at the sub-microscopic scale, the effective creep compliance was obtained by applying the Ricaud and Masson formula [49] that relates the viscoelastic coefficients of a porous composite (k_{f_p}) with the volume fractions of the pores (f_p):

$$k_{f_p} = k_{car} \frac{4}{3A(f_p)} \tag{23}$$

where $A(f_p) = \dfrac{f_p}{1 - f_p}$.

Here, we considered this formula for the matrix of cement paste when k_{f_p} represents the viscoelastic coefficient of C-S-H. Thus, at the cement paste scale, by knowing the creep compliance of the matrix $J_{CSHP}(t)$, the effective creep compliance of cement paste J_p^{hom} could be calculated by the homogenization method. Then we went up to the mortar scale, and finally to the concrete scale.

5. Determination of the viscoelastic parameters

5.1. Characteristic viscoelastic coefficients of C-S-H

The calibration procedure began by the concrete scale in order to reproduce the delayed displacement curves of concrete C-N-N, and then descended successively to the C-S-H scale. First, at the concrete scale, the Young's modulus E and the tensile strength f_t of both the mortar and aggregate were already determined in Guo et al. [3]. Then, at the mortar scale, the Young's modulus of the cement paste was calculated according to a hydration model [50], and the tensile strength was calibrated by simulating uniaxial tension tests of mortar. The Young's modulus and the tensile strength of sand grains were taken from the literature [34]. At the cement paste scale, the Young's modulus of the matrix (C-S-H + capillary pores) was calculated according to Mori-Tanaka's homogenization method. The tensile strength of the matrix was calibrated by simulating uniaxial tension tests of cement paste. The Young's modulus of inclusions was calculated by averaging the Young's modulus of each component of the $V_{hy-clinkers}$ set. Their tensile strength was derived from the literature [34]. All the parameters determined here are summarized in Table 2.

Table 2: Young's modulus and tensile strength of the constituents of each scale.

		f_t(MPa)	E(GPa)
Concrete (C-N-N)	Mortar	1.6	27.45
	Aggregate	6	78
Mortar	Cement paste	1.5	14.34
	Sand grain	8	80
Cement paste	Matrix of the paste	1.4	8.18
	Inclusion of the paste	3	51.6

Considering the creep-loading period (three months), four chains of Kelvin-Voigt were taken into account, corresponding respectively to the characteristic time of 0.1, 1, 10 and 100 days. Then, at the concrete scale, the viscoelastic coefficients of mortar were identified by minimizing the difference between the calculated specific delayed displacement and the measured one (Figure 6). The identification of these parameters made it possible to calculate the creep compliance of mortar $J_m(t)$ by using the expression of $J_{ijkl}(t)$ (equation (16)).

At the mortar scale, the viscoelastic parameters of the cement paste were adjusted to obtain the compliance of mortar $J_m^{hom}(t)$, which was equivalent to $J_m(t)$ as determined in the previous step (Figure 6). The identified parameters were used to calculate the creep compliance of cement paste $J_p(t)$.

At the cement paste scale, the viscoelastic parameters of the paste's matrix $J_{CSHP}(t)$ were calibrated to get the compliance of the paste $J_p^{hom}(t)$, identical to $J_p(t)$ as defined in the last step (Figure 6). All the identified parameters are recapitulated in Table 3. Note that creep deformation for inclusions at each scale was considered as equal to zero, which corresponds to a very high coefficient value.

Table 3: Viscoelastic parameters of the constituents of each scale.

		k_v^1 (GPa)	k_v^2(GPa)	k_v^3(GPa)	k_v^4(GPa)
Concrete (C-N-N)	Mortar	90	45	22	4
	Aggregate	1×10^{30}	1×10^{30}	1×10^{30}	1×10^{30}
Mortar	Cement paste	48	19	8	1.7
	Sand grain	1×10^{30}	1×10^{30}	1×10^{30}	1×10^{30}
Cement paste	Paste matrix	25	9	4	0.8
	Inclusion of paste	1×10^{30}	1×10^{30}	1×10^{30}	1×10^{30}

The viscoelastic parameters of the cement paste matrix identified above were dependent on the porosity of concrete. The coefficients $k_{f_p}^i$ are associated with the i chain of the Kelvin model. According to Ricaud and Masson [49], the viscoelastic coefficients of a porous medium are related to the characteristic coefficients which are independent of the porosity and represent only the solid phase (equation 23). For concrete C-N-N, the volume fraction of pores calculated by the hydration model is 34 % of the cement paste volume; thus f_p is equal to 46.9 % at the C-S-H scale. The values of the Kelvin characteristic coefficients of C-S-H (the cement paste matrix) were calculated according to the Ricaud and Masson formula and the corresponding results are presented in Table 4.

5.2. Calculation of the viscoelastic parameters of EI

In the case of RAC, the EI around recycled aggregate is composed of not only the new interfacial transition zone (ITZ) but also the old ITZ and the old residual mortar. However, it is usually

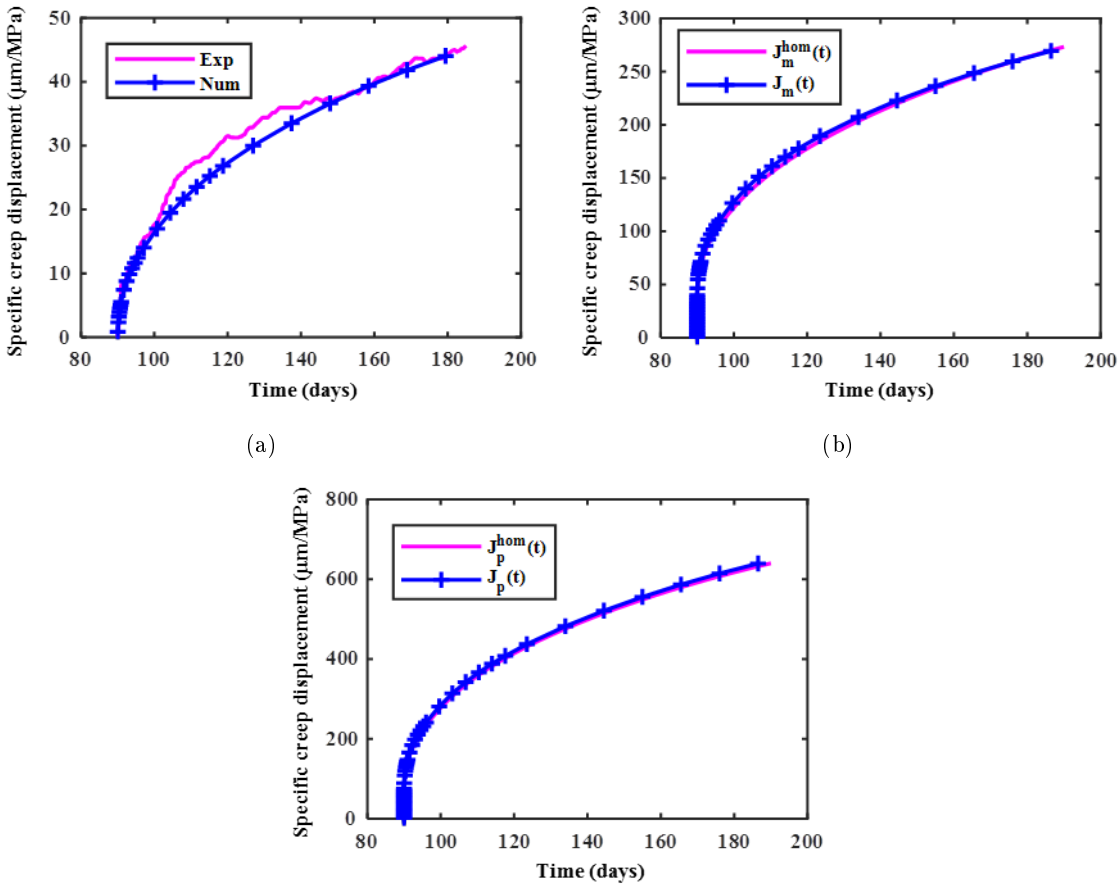

Figure 6: (a) Comparison between the experimental delayed specific displacement of concrete C-N-N and the identified numerical one, (b) comparison between the compliance $J_m(t)$ and the identified compliance $J_m^{hom}(t)$ at the mortar scale, (c) comparison between the compliance $J_p(t)$ and the identified compliance $J_p^{hom}(t)$ at the scale of cement paste.

Table 4: Characteristic viscoelastic coefficients of Kelvin for the matrix of cement paste.

k_{car}^1(GPa)	k_{car}^2(GPa)	k_{car}^3(GPa)	k_{car}^4(GPa)
16.56	5.96	2.65	0.53

observed that with the aging of concrete, the ITZ tends to have the same properties as the cement mortar near this zone; the differences in mechanical strength also reduce gradually with time. The microcracking origins identified from the multiparametric clustering of acoustic emission signals recorded during flexural tests were aggregate fracture, cracking in the old residual mortar and cracking in the mortar matrix [3], which confirms the observation mentioned above. Thus in our modeling, we chose to not distinguish the old ITZ within the old attached mortar by assigning them the same properties. Furthermore, in order to limit the uncertainties about the local properties, we did not adjust for the new aggregate-matrix ITZ. Consequently, in this work the EI surrounding recycled aggregate is considered to be composed of a layer of old mortar and a layer of new mortar. The thickness of the EI is chosen to be 100 µm so as to complete the simulation within an acceptable time [42].

As demonstrated in the previous work of the authors [36], the properties of old attached mortar have a non-negligible effect on the macroscopic mechanical behavior of recycled concrete and need to be properly defined. Since it is very difficult to define the real content of old mortar in EI, the authors considered five composition possibilities of EI [51, 52], i.e., 10 %, 20 %, 30 %, 40 % and 50 % old mortar with the corresponding 90 %, 80 %, 70 %, 60 % and 50 % new mortar, respectively, to characterize the influence of old mortar content on the global mechanical behavior of concrete. The modeling results of fracture tests showed that the most reasonable component of EI for our case of study was 20 % old mortar and 80 % new mortar [36]. Certainly the old adhered mortar content varies with the waste material origin. However, the same methodology can be used with minor adjustments to determine the EI fractional component for other types of RAC, by calibrating with certain experimental tests.

In order to represent the properties of unknown old attached mortar that is composed of unknown cement paste as matrix and sand as inclusion, four types of ordinary cement paste (w/c=0.4, 0.5, 0.6 and 0.65) were studied. First, at the cement paste scale, the viscoelastic parameters of the four types of cement paste were determined by calculating the volume fraction of the pores f_p in the cement paste's matrix according to the hydration model. Simultaneously, for each type of paste, the Young's modulus of its matrix (C-S-H + capillary pores) was calculated based on Mori-Tanaka's

homogenization method. The Young's modulus of the inclusions was obtained by averaging that of each component of the set $V_{hy-clinkers}$. All the results are summarized in Table 5.

Table 5: Elastic parameters for the four types of cement paste.

w/c		0.4	0.5	0.6	0.65
	f_p	0.14	0.313	0.426	0.469
Matrix of cement paste	E (GPa)	16.45	11.61	9.05	8.18
	ν	0.26	0.28	0.29	0.3
Inclusion of cement paste	E (GPa)	53.09	52.9	52.19	51.6
	ν	0.31	0.31	0.31	0.31

Note that the parameters vary with the w/c ratio, except the Poisson's ratio of the inclusion. For the purpose of representing the range of the elastic parameters, the cement pastes with w/c equal to 0.4 (minimum) and 0.65 (maximum) were taken into account in the following simulation. Moreover, the viscoelastic parameters of the maximum group had already been determined, as discussed in the previous section. Thus, only the properties of the minimum group remained to be determined.

As mentioned above, the viscoelastic parameters of the cement paste's matrix were calculated according to the equation (23). Then the compliance of the cement paste J_p^{hom} was determined by the numerical homogenization method (Figure 7) as a constant load of 40 % of the maximal strength was applied at the age of three months. The instantaneous part was removed when the desired force was reached. By minimizing the difference between the homogenized compliance and the calculated one (formula (16)), the viscoelastic parameters of Kelvin model k_v^i for cement paste at different ages were identified according to the least square method.

The identification of k_v^i for cement pastes made it possible to calculate the homogenized creep compliance J_m^{hom} at the mortar scale (Figure 7). Then the viscoelastic parameters k_v^i of the mortar were determined. Table 6 shows the calculated and retained values for scales from C-S-H to mortar. The inclusions' effect on the viscosity of the material is noted here since, for example, the compliance of mortar is inferior to that of the cement paste, due to the presence of sand grains.

As the viscoelastic parameters of new mortar were determined in the previous section, the

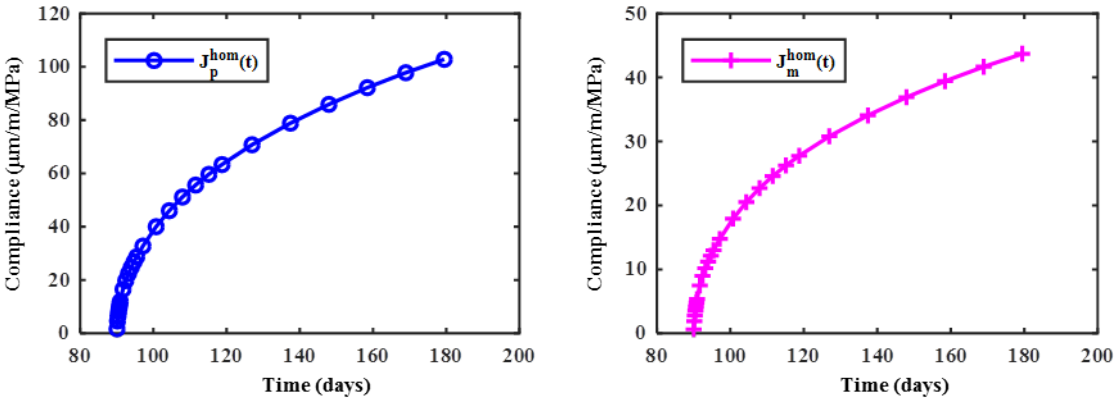

(a) (b)

Figure 7: (a) Creep compliance of cement paste, (b) creep compliance of mortar.

Table 6: Viscoelastic parameters of the matrices for the three scales.

	k_v^1 (GPa)	k_v^2(GPa)	k_v^3(GPa)	k_v^4(GPa)
Matrix of cement paste	135.64	48.83	21.70	4.34
Cement paste	369.98	86.84	39.62	9.31
Mortar	892.43	203.62	97.88	21.61

viscoelasticity of the EI (both the minimum and the maximum groups) was obtained by averaging the viscoelastic parameters of its components ($k_v^{au} = 0.2k_v^{old} + 0.8k_v^{new}$). The retained values are listed in Table 7. The viscoelasticity of the homogeneous parts of the beam was considered identical to that of new mortar, since the stiffness and the viscoelasticity of the extreme zones do not have a great influence on the overall creep displacement. Thus the parameters in these zones can be arbitrarily defined as close to those of a viscoelastic material, which is very similar to concrete. Here we took directly the viscoelastic parameters of the mortar; it can be verified that the results do not change with higher stiffness.

Table 7: Viscoelastic parameters of all the considered phases in beam C-N-100R.

	k_v^1 (GPa)	k_v^2(GPa)	k_v^3(GPa)	k_v^4(GPa)
Mortar	90	45	22	4
Recycled aggregate	1×10^{30}	1×10^{30}	1×10^{30}	1×10^{30}
Interphase (min)	250.49	76.72	37.18	7.52
Interphase (max)	90	45	22	4
Homogeneous concrete	90	45	22	4

Based on all the available parameters, the numerical simulation was carried out. The obtained specific delayed displacements are shown in Figure 8 in comparison with the experimental result. Note that the numerical values are less than those of the experiment. In order to understand this difference, a review of the whole modeling process was conducted. Until now, the influence of 100 % RA on the creep displacement of concrete has been taken into account by the identification of viscoelastic parameters of the interphase between RA and the new forming mortar. These parameters were calculated from the characteristic coefficients of C-S-H by passing through the scales of cement paste and mortar. The only difference of the assumed old cement paste and the new one is the volume fraction of the pores f_p in the cement paste's matrix. In this work, f_p of the old cement paste was less than that of the new cement paste, which is consistent with the findings of Li et al. [53] that the rehydration of old cement paste reduces its porosity. Actually, the difference of f_p is not sufficient to explain the increment of the RAC's creep deformation. Furthermore, several studies [54, 55] have shown that the RAs themselves have a higher porosity as well as a higher water

absorption ratio, and are less resistant to shock and friction [29]. The aggregates' porosity affects the elastic modulus and thus indirectly affects concrete creep. As the aggregates' elastic moduli decrease, there is greater stress on the cement paste and thus greater creep [28]. So the viscoelastic strain of RAs should be taken into account in the simulation. After being verified several times, $k_v^{ra} = 23\,\text{GPa}$ was assigned to represent the viscoelasticity of RA.

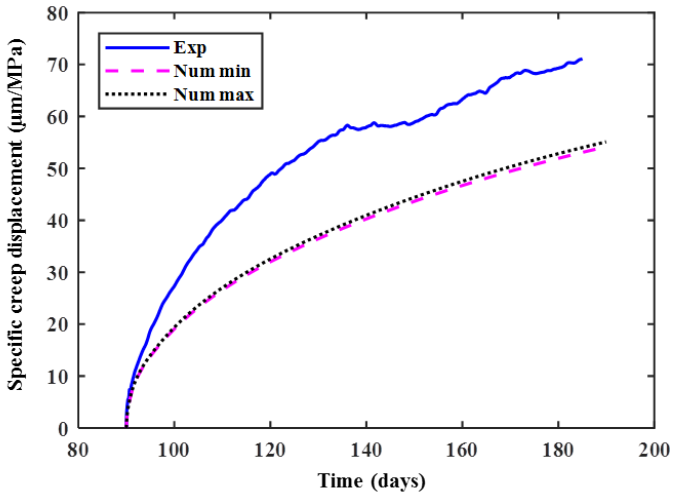

Figure 8: Comparison of the numerical specific creep displacement with the experimental one for beam C-N-100R.

Remind that the viscoelastic parameters in the maximum group of the interphase were chosen for the following simulation, which implies that the maximum creep displacement was considered in this study. The new numerical curve calculated by considering k_v^{ra} is presented in Figure 9. Further verification by other types of concrete with different RA replacement ratios is needed in order to verify the introduction of the viscoelasticity of RA.

6. Verification of the proposed model

All the identified viscoelastic parameters and the corresponding methods used in the previous section are summarized in Table 8. The verification of these parameters, without any other adjustment, was carried out by performing the simulation of the creep test of C-N-30R.

The obtained results are presented in Figure 10. We notice that the numerical curve is very close to the experimental one, which implies that the inverse analysis of the viscoelastic parameters is

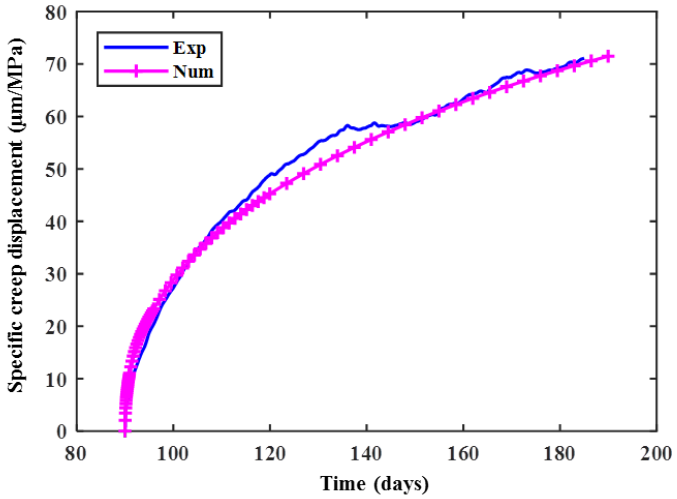

Figure 9: Specific creep displacement of beam C-N-100R by considering the creep of recycled aggregate.

Table 8: Viscoelastic parameters determined for the three scales.

Concrete type	Scale	Constituent	Identification method
C-N-N	Concrete	Mortar	Calibrated
		Aggregate	Imposed
	Mortar	Cement paste	Calibrated
		Sand grain	Imposed
	Cement paste	Matrix	Calibrated
		Inclusion	Imposed
C-N-100R	Concrete	Mortar	Calibrated
		Aggregate	Imposed
		Interphase	Multi-scale model
	Mortar	Cement paste	Multi-scale model
		Sand grain	Imposed
	Cement paste	Matrix	Multi-scale model
		Inclusion	Imposed

reliable and the determined parameters can be used to estimate the actual creep evolution of RAC. In particular, the viscoelasticity of RA was an influential factor in reproducing the experimental creep behavior of RAC. Thus, the validated model can be exploited to identify the cracking risk during creep.

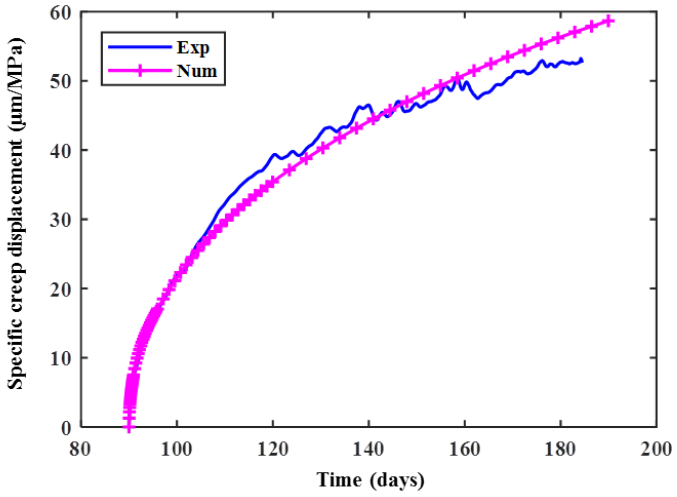

Figure 10: Comparison of the numerical specific creep displacement curve with that of the experiment for C-N-30R.

7. Damage evolution in concrete microstructure

After three months of loading at a stress level of 40 % of the maximal strength, the damage localization field of beam C-N-100R was calculated (Figure 11). For comparison, the damage localization map at the 40 % pre-peak loading step during the fracture test is also presented in Figure 11. Note that the damage localized in front of the notch, and developed mainly in the mortar matrix as well as in the interphase. As the RAs are less resistant, cracks were found to propagate through the aggregate. This phenomenon corresponds to our hypothesis that the effect of RA on the creep evolution of RAC is not negligible. In fact, after three months of constant loading, the failure behavior of C-N-100R was found to be more fragile during the post-peak region, though the flexural strength varied very little after creep [36] (Figure 12).

Similarly, the damage localization field of beam C-N-30R after three months of loading was also calculated and compared with the damage state before the constant loading of creep (Figure 11).

We observed that the cracks were located above the notch and propagated toward the top of the beam by passing around the aggregate that hindered them. Damage was principally found in the matrix and in the interphase around the RAs. For the fracture behavior of concrete with 30 % recycled aggregate after three months of loading, similar trends were observed by comparison with that before creep [36] (Figure 12).

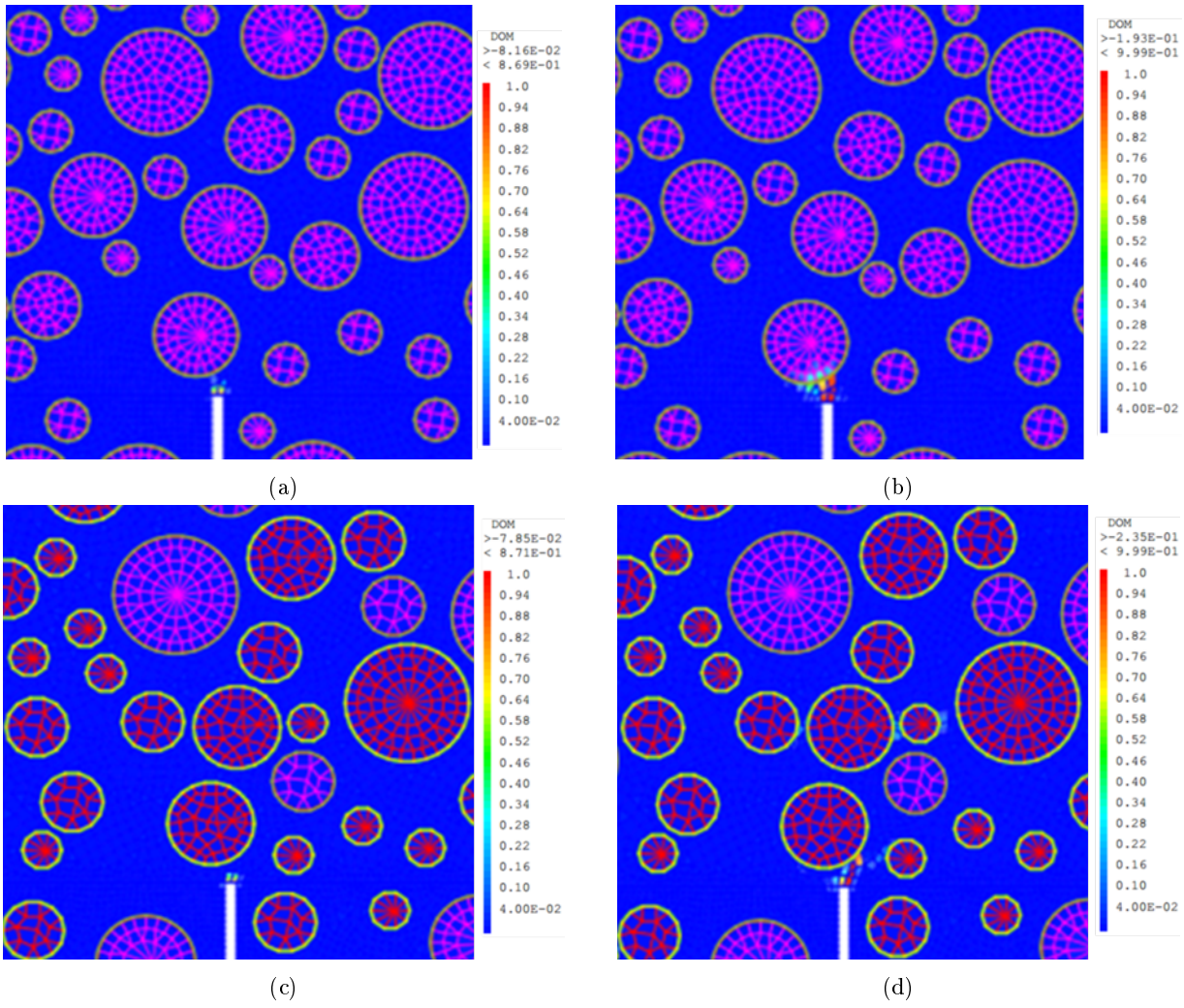

Figure 11: Damage localization fields of beams (a) C-N-100R at 40 % pre-peak loading step during fracture, (b) C-N-100R after three months of loading at a stress level of 40 % F_{max}, (c) C-N-30R at 40 % pre-peak loading step during fracture, (d) C-N-30R after three months of loading at a stress level of 40 % F_{max}.

Based on the established model, we also calculated the creep displacement for other types

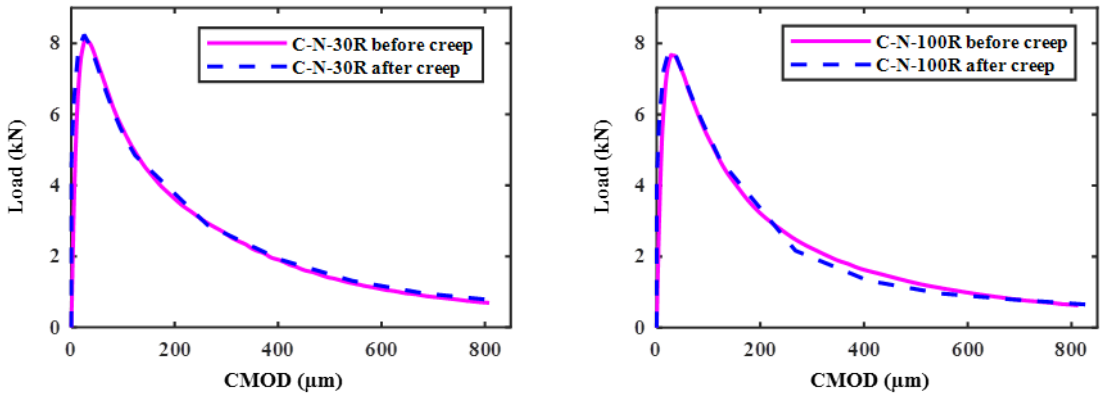

(a) (b)

Figure 12: Comparison of the Load-CMOD curves before and after three months of constant loading for (a) C-N-30R, (b) C-N-100R.

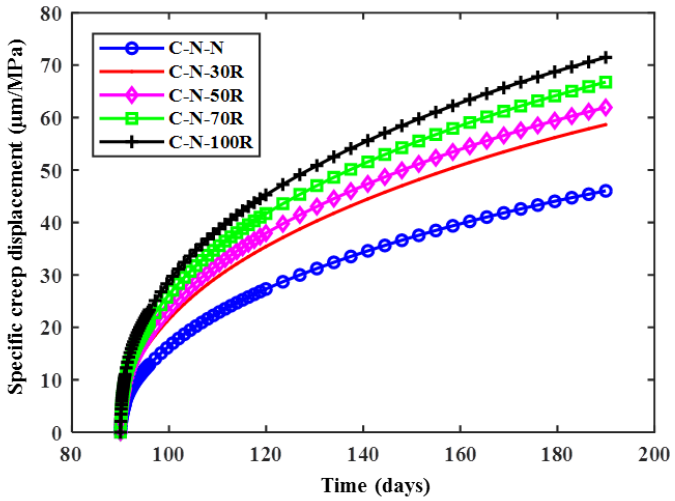

Figure 13: Identified numerical creep displacement curves for different types of recycled aggregate concrete.

of RAC, for example C-N-50R and C-N-70R, by applying the virtual aggregate size distribution respectively (Figure 13). We noted that the creep displacement increased with the substitution ratio of natural aggregate by RAs, as demonstrated in the literature [12, 14]. We concluded that the proposed model has a certain capacity to predict the creep behavior of RAC on the basis of the identified viscoelastic parameters for new mortar, old attached mortar and RAs. In addition, by using the creep-damage coupling model, the microcracks generated during the constant loading period that were almost impossible to measure by experimental methods could be detected. The influence of the constituent phases on the delayed behavior of concrete could be explicitly illustrated.

8. General remarks

Normally, it takes at least six months to complete the creep test, whereas with the proposed creep model we were able to obtain RAC creep evolution information after only a few hours of computation. The efficiency of numerical modeling is evident in the study of long-term RAC mechanical behavior. Furthermore, we were able to calculate the viscoelastic properties of any type of RAC at different ages by applying the cement hydration model [50]. Creep tests of any type of RAC specimens subjected to different stress levels can also be modeled for a desired loading period.

Generally, the creep behavior of concrete is considered to be linear under a stress level of 40 % of the maximal strength. However, that is not necessarily the case for C-N-100R. As shown in Figure 11, the damage developed in front of the notch during creep. Further research work is needed in order to study and evaluate the creep-damage coupling of RAC in the long term.

Due to the fact that the creep behavior of RAC is highly influenced by origin of RAs, mixture design of new concrete, specimen size, loading mode, temperature and relative humidity during the test, certain adjustment is surely needed and could be realized for the actual application of this numerical method in other creep-related studies. The methodology proposed here could serve as a useful reference for the prediction of RAC creep.

9. Conclusions

The creep behavior of three types of recycled aggregate concrete was studied on three-point bending beams subjected to a stress level of 40 % of the maximal strength over a period of three

months. The delayed displacement of concrete increased with the replacement ratio of natural aggregate by recycled aggregate. A micro-macro modeling of the creep test was carried out to investigate the roles of the different phases on the creep behavior of recycled aggregate concrete. The following conclusions were drawn:

- The creep kinetics of 30 % recycled aggregate concrete were comparable to those of normal concrete with an amplitude 1.2 times greater after three months of loading. For concrete with 100 % recycled aggregate, the creep developed faster and the amplitude was 1.6 times larger than that of conventional concrete.

- The simulation results showed that the time-dependent behavior of recycled aggregates themselves was not negligible and should be taken into account in numerical modeling. The greater contribution of recycled aggregate on the development of the delayed displacement of concrete needs to be considered in the future application of recycled concrete structures.

- According to the damage localization maps of recycled concrete, the microcracks developed not only in the mortar matrix and the interphase but also in the recycled aggregate, due to its higher porosity and lower particle strength. This implies that the commonly considered linear creep of concrete under a stress level of 40 % of the maximal strength is not absolutely the case for recycled aggregate concrete. Further studies are essential in order to facilitate the wider application of recycled aggregate in structural concrete.

In addition, a similar work to model the creep behavior of recycled aggregate by using the downscaling analysis is currently under way. The difference lies at the cement paste scale where, instead of homogenizing the heterogeneous matrix and inclusions of the cement paste, the real microstructure, composed of all the existing clinker minerals phases and the hydration products, is considered. The influence of the microscopic components on the creep behavior of recycled aggregate concrete will be presented in the next paper.

Acknowledgments

Support from the French National Research Agency (ANR: Agence Nationale de la Recherche) is acknowledged (ECOREB project). The first author would like to thank the China Scholarship Council for the financial support (PhD grant).

References

[1] R. Silva, J. De Brito, R. Dhir, Properties and composition of recycled aggregates from construction and demolition waste suitable for concrete production, Construction and Building Materials 65 (2014) 201–217.

[2] N. Tošić, S. Marinković, I. Ignjatović, A database on flexural and shear strength of reinforced recycled aggregate concrete beams and comparison to Eurocode 2 predictions, Construction and Building Materials 127 (2016) 932 – 944.

[3] M. Guo, S. Y. Alam, A. Z. Bendimerad, F. Grondin, E. Rozière, A. Loukili, Fracture process zone characteristics and identification of the micro-fracture phases in recycled concrete, Engineering Fracture Mechanics 181 (2017) 101–115.

[4] Z. Zhao, S. Remond, D. Damidot, W. Xu, Influence of fine recycled concrete aggregates on the properties of mortars, Construction and Building Materials 81 (2015) 179–186.

[5] J. Xiao, W. Li, Y. Fan, X. Huang, An overview of study on recycled aggregate concrete in China (1996–2011), Construction and Building Materials 31 (2012) 364–383.

[6] G. Wardeh, E. Ghorbel, H. Gomart, Mix design and properties of recycled aggregate concretes: applicability of Eurocode 2, International Journal of Concrete Structures and Materials 9 (1) (2015) 1–20.

[7] N. Tošić, S. Marinković, T. Dašić, M. Stanić, Multicriteria optimization of natural and recycled aggregate concrete for structural use, Journal of Cleaner Production 87 (2015) 766–776.

[8] Eurocode 2: Design of Concrete Structures: Part 1-1: General Rules and Rules for Buildings, British Standards Institution, 2004.

[9] Z. P. Bazant, F. H. Wittmann, Creep and shrinkage in concrete structures, Wiley New York, 1982.

[10] C.-Q. Lye, R. K. Dhir, G. S. Ghataora, H. Li, Creep strain of recycled aggregate concrete, Construction and Building Materials 102 (2016) 244–259.

[11] N. Tošić, S. Marinković, N. Pecić, I. Ignjatović, J. Dragaš, Long-term behaviour of reinforced beams made with natural or recycled aggregate concrete and high-volume fly ash concrete, Construction and Building Materials 176 (2018) 344 – 358.

[12] A. Domingo-Cabo, C. Lázaro, F. López-Gayarre, M. Serrano-López, P. Serna, J. O. Castaño-Tabares, Creep and shrinkage of recycled aggregate concrete, Construction and Building Materials 23 (7) (2009) 2545–2553.

[13] S. Seara-Paz, B. González-Fonteboa, F. Martínez-Abella, I. González-Taboada, Time-dependent behaviour of structural concrete made with recycled coarse aggregates. Creep and shrinkage, Construction and Building Materials 122 (2016) 95–109.

[14] V. W. Tam, D. Kotrayothar, J. Xiao, Long-term deformation behaviour of recycled aggregate concrete, Construction and Building Materials 100 (2015) 262–272.

[15] Y. Wang, Q. Wang, Y. Geng, G. Ranzi, Long-term behaviour of simply supported composite slabs with recycled coarse aggregate, Magazine of Concrete Research 68 (24) (2016) 1278–1293.

[16] A. M. Knaack, Y. C. Kurama, Creep and Shrinkage of Normal-Strength Concrete with Recycled Concrete Aggregates., ACI Materials Journal 112 (3).

[17] Y. Fan, J. Xiao, V. W. Tam, Effect of old attached mortar on the creep of recycled aggregate concrete, Structural Concrete 15 (2) (2014) 169–178.

[18] S.-C. Kou, C.-S. Poon, M. Etxeberria, Influence of recycled aggregates on long term mechanical properties and pore size distribution of concrete, Cement and Concrete Composites 33 (2) (2011) 286–291.

[19] F. Cartuxo, J. De Brito, L. Evangelista, J. R. Jimenez, E. Ledesma, Rheological behaviour of concrete made with fine recycled concrete aggregates–Influence of the superplasticizer, Construction and Building Materials 89 (2015) 36–47.

[20] Y. Geng, Y. Wang, J. Chen, Creep behaviour of concrete using recycled coarse aggregates obtained from source concrete with different strengths, Construction and Building Materials 128 (2016) 199–213.

[21] C. S. Poon, Z. Shui, L. Lam, Effect of microstructure of ITZ on compressive strength of concrete prepared with recycled aggregates, Construction and Building Materials 18 (6) (2004) 461–468.

[22] J. Xiao, W. Li, Z. Sun, D. A. Lange, S. P. Shah, Properties of interfacial transition zones in recycled aggregate concrete tested by nanoindentation, Cement and Concrete Composites 37 (1) (2013) 276–292.

[23] G. Fathifazl, A. Razaqpur, Creep Rheological Models for Recycled Aggregate Concrete., ACI Materials Journal 110 (2).

[24] G. Fathifazl, A. G. Razaqpur, O. B. Isgor, A. Abbas, B. Fournier, S. Foo, Creep and drying shrinkage characteristics of concrete produced with coarse recycled concrete aggregate, Cement and Concrete Composites 33 (10) (2011) 1026–1037.

[25] R. Recommendation, Specifications for concrete with recycled aggregates, Materials and Structures 27 (173) (1994) 557.

[26] A. Domingo, C. Lazaro, F. L. Gayarre, M. Serrano, C. Lopez-Colina, Long term deformations by creep and shrinkage in recycled aggregate concrete, Materials and structures 43 (8) (2010) 1147–1160.

[27] M. Bravo, J. de Brito, J. Pontes, L. Evangelista, Durability performance of concrete with recycled aggregates from construction and demolition waste plants, Construction and Building Materials 77 (2015) 357–369.

[28] R. Silva, J. De Brito, R. Dhir, Comparative analysis of existing prediction models on the creep behaviour of recycled aggregate concrete, Engineering Structures 100 (2015) 31–42.

[29] S. Omary, E. Ghorbel, G. Wardeh, Relationships between recycled concrete aggregates characteristics and recycled aggregates concretes properties, Construction and Building Materials 108 (2016) 163–174.

[30] L. Evangelista, J. De Brito, Durability performance of concrete made with fine recycled concrete aggregates, Cement and Concrete Composites 32 (1) (2010) 9–14.

[31] A. Bendimerad, E. Roziere, A. Loukili, Combined experimental methods to assess absorption rate of natural and recycled aggregates, Materials and Structures 48 (11) (2015) 3557–3569.

[32] M. Casuccio, M. Torrijos, G. Giaccio, R. Zerbino, Failure mechanism of recycled aggregate concrete, Construction and Building Materials 22 (7) (2008) 1500–1506.

[33] J. Saliba, F. Grondin, M. Matallah, A. Loukili, H. Boussa, Relevance of a mesoscopic modeling for the coupling between creep and damage in concrete, Mechanics of time-dependent materials 17 (3) (2013) 481–499.

[34] M. Farah, Développement d'un modèle multi-échelles et d'une procédure expérimentale pour l'analyse du couplage fluage-endommagement du béton au jeune âge, Ph.D. thesis, Ecole Centrale de Nantes, 2015.

[35] M. Omar, A. Loukili, G. Pijaudier-Cabot, Y. Le Pape, Creep-damage coupled effects: experimental investigation on bending beams with various sizes, ASCE journal of Materials in Civil Engineering 21 (2) (2009) 65–72.

[36] M. Guo, F. Grondin, A. Loukili, Numerical analysis of the failure of recycled aggregate concrete

by considering the random composition of old attached mortar, Building and Environment, Submitted .

[37] V. Šmilauer, Z. P. Bažant, Identification of viscoelastic CSH behavior in mature cement paste by FFT-based homogenization method, Cement and Concrete Research 40 (2) (2010) 197–207.

[38] J. M. Torrenti, R. Leroy, Analyse et modélisation du fluage propre du béton, in: Rencontres Universitaires de Génie Civil, 2015.

[39] Q. H. Do, S. Bishnoi, K. L. Scrivener, Microstructural modeling of early-age creep in hydrating cement paste, Journal of Engineering Mechanics 142 (11) (2016) 04016086.

[40] K. Velez, S. Maximilien, D. Damidot, G. Fantozzi, F. Sorrentino, Determination by nanoindentation of elastic modulus and hardness of pure constituents of Portland cement clinker, Cement and Concrete Research 31 (4) (2001) 555–561.

[41] M. Vandamme, F.-J. Ulm, Nanogranular origin of concrete creep, Proceedings of the National Academy of Sciences 106 (26) (2009) 10552–10557.

[42] F. Grondin, M. Matallah, How to consider the Interfacial Transition Zones in the finite element modelling of concrete?, Cement and Concrete Research 58 (2014) 67–75.

[43] F. Grondin, H. Dumontet, A. B. Hamida, G. Mounajed, H. Boussa, Multi-scales modelling for the behaviour of damaged concrete, Cement and Concrete Research 37 (10) (2007) 1453–1462.

[44] G. Mounajed, Exploitation du nouveau modèle béton numérique dans symphonie: Concept, homogénéisation du comportement thermomécanique des BHP et simulation de l'endommagement thermique, Cahiers du CSTB, Centre Scientifique et Technique du Bâtiment, 2002.

[45] S. Fichant, G. Pijaudier-Cabot, C. La Borderie, Continuum damage modelling: approximation of crack induced anisotropy, Mechanics Research Communications 24 (2) (1997) 109–114.

[46] S. Fichant, C. La Borderie, G. Pijaudier-Cabot, Isotropic and anisotropic descriptions of damage in concrete structures, Mechanics of Cohesive-frictional Materials 4 (4) (1999) 339–359.

[47] N. Reviron, F. Benboudjema, J.-M. Torrenti, G. Nahas, A. Millard, Coupling between creep and cracking in tension, in: Framcos 6th International Conference on Fracture Mechanics of Concrete and Concrete Structures, vol. 6, Catania, 495–502, 2007.

[48] F. Grondin, Modélisation multi-échelles du comportement thermo-hydro-mécanique des matériaux hétérogènes applications aux matériaux cimentaires sous siolicitations sévères., Ph.D. thesis, Université Paris 6, 2005.

[49] J.-M. Ricaud, R. Masson, Effective properties of linear viscoelastic heterogeneous media: Internal variables formulation and extension to ageing behaviours, International Journal of Solids and Structures 46 (7) (2009) 1599–1606.

[50] F. Grondin, M. Bouasker, P. Mounanga, A. Khelidj, A. Perronnet, Physico-chemical deformations of solidifying cementitious systems: multiscale modelling, Materials and Structures 43 (1-2) (2010) 151–165.

[51] A. Elsharief, M. D. Cohen, J. Olek, Influence of aggregate size, water cement ratio and age on the microstructure of the interfacial transition zone, Cement and Concrete Research 33 (11) (2003) 1837 – 1849.

[52] K. L. Scrivener, A. K. Crumbie, P. Laugesen, The interfacial transition zone (ITZ) between cement paste and aggregate in concrete, Interface Science 12 (4) (2004) 411–421.

[53] T. Li, J. Xiao, C. Zhu, Hydration process modeling of ITZ between new and old cement paste, Construction and Building Materials 109 (2016) 120–127.

[54] A. Gutiérrez, E. Vázquez, C. F. Hendriks, G. Janssen, Influence of attached mortar content on the properties of recycled concrete aggregate, in: International RILEM Conference on the Use of Recycled Materials in Building and Structures, RILEM Publications SARL, 536–544, 2004.

[55] S. H. Kosmatka, W. C. Panarese, B. Kerkhoff, Design and control of concrete mixtures, Portland Cement Association Skokie, IL .